MATHEMATICAL MODELING AND COMPUTING, Vol. 10, No. 2, pp. 410–420 (2023)

A numerical evaluation of the temperature of a solidification point in ingot casting processes

Zambrano M.

Universidad Nacional de Barranca,
Barranca, 15169, Lima, Peru

(Received 17 June 2022; Accepted 18 April 2023)

An analysis for the numerical computing of the temperature around a solidification point of liquid steel or melt contained in a mould is performed via the interaction of the conservation equations of mass, momentum and heat transfer. A cooling process of liquid steel due to the extraction of heat through the walls of the mould is analyzed using asymptotic methods and an ordinary differential equation that describes the temperature of interface melt-air is obtained. Also, the temperature of the melt in the mould around the solidification point is computed numerically using the OpenFOAM software.

Keywords: *solidification point; cooling process; asymptotic methods; ordinary differential equation.*

2010 MSC: 35Q79 **DOI:** 10.23939/mmc2023.02.410

1. Introduction

In steelmaking industry, *ingot casting* is a process to produce ingots inside a static mould. In the process, liquid steel is poured into a mould wherein a cooling process occurs by extracting heat through the walls of the mould and to obtain the solid steel product. Usually, small indentations are observed on the surface of the solid steel which is considered a defect and it is referred to as *ripple marks* [1–4] and to become interesting to know how this defect can be avoided.

Although the mechanism of formation of ripple marks depends on the properties of the liquid steel, it is interesting to analyze a cooling process which leads to the solidification of steel [5, 6], and hence to obtain some insights in how to prevent its formation by avoiding the solidification of the existing melt in the mould.

Likewise, the mathematical modeling of this cooling process can be regarded as a starting point to understand the cooling mechanism of more complex models with the purpose to avoid defects in the steelmaking industry as that found in continuous casting where a combination of cooling of liquid steel and oscillation of the mould produces a defect on the surface of the final product known as *oscillation marks* [6–9].

An alternative to avoid this unwanted defect has been proposed by Vynnycky et al. [1], which is based on the idea of finding the relation between the casting velocity and casting temperature of the steel so that the onset of the solidification of the steel inside of the mould is initiated once the mould is filled up. In this proposal plays a important role the existence of a point referred to as *triple point* where three interfaces: mould wall-air, air-melt and melt-mould wall meet and where melt is at its lowest temperature [1].

In this research, the cooling process around this triple point, also known as *solidification point* [1] is investigated through of the temperature of the liquid steel filling a mould according to the configuration given by Tomono [3] and Schwerdtfeger [8]. Likewise, it is analyzed the temperature on the rising interface between the melt and the air in the mould referred to as *meniscus* and whose shape is consequence of the surface tension [10].

2. Model equations

In a channel-shaped mould with walls are a distance $2W$ apart and height is L, liquid steel at casting temperature T_c enters with casting velocity V_c and forms a meniscus where profile is given by $y = h(x,t)$, x, y denote the horizontal and vertical coordinates respectively and t denotes the time; initially at $t = 0$, this profile is given by $y = y_0$. This situation is depicted in Figure 1 wherein $\tilde{p}$ indicates the solidification point and at the mould wall Q is the heat flux released in this cooling process.

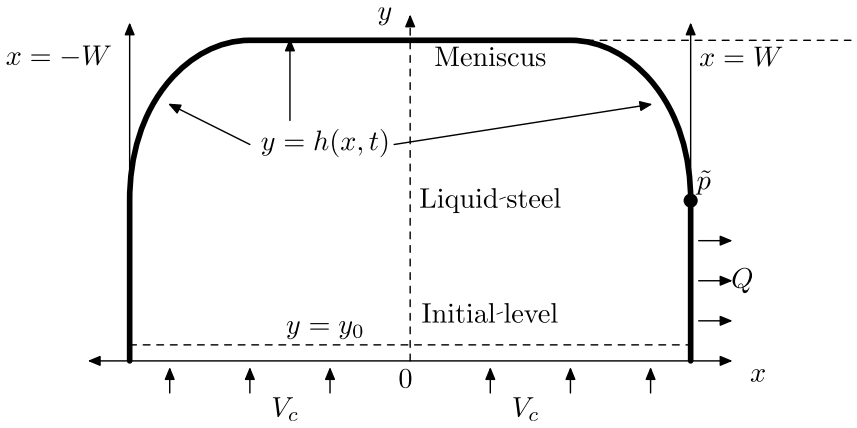

Fig. 1. Schematic of the meniscus whose profile is given by $h = h(x,t)$, and initially is $y = y_0$. As the melt enters to the mould with a constant velocity V_c, a heat flux Q at the wall $x = W$ is released by the mould wall.

The horizontal and vertical components of the fluid flow velocity inside the mould are denoted by u and v respectively and the pressure denoted by p; also, the density and viscosity of the melt are denoted by ρ and μ respectively. Thus, the mass and momentum conservation equations for the fluid flow [11, 12] are given by

$$\frac{\partial u}{\partial x} + \frac{\partial v}{\partial y} = 0, \tag{1}$$

$$\rho\left(\frac{\partial u}{\partial t} + u\frac{\partial u}{\partial x} + v\frac{\partial u}{\partial y}\right) = -\frac{\partial p}{\partial x} + \mu\left(\frac{\partial^2 u}{\partial x^2} + \frac{\partial^2 u}{\partial y^2}\right), \tag{2}$$

$$\rho\left(\frac{\partial v}{\partial t} + u\frac{\partial v}{\partial x} + v\frac{\partial v}{\partial y}\right) = -\frac{\partial p}{\partial y} + \mu\left(\frac{\partial^2 v}{\partial x^2} + \frac{\partial^2 v}{\partial y^2}\right) - \rho\, g, \tag{3}$$

where g is the gravity constant. Likewise, the temperature T of the liquid steel is governed by heat transfer equation given by

$$\rho\, c_p\left(\frac{\partial T}{\partial t} + u\frac{\partial T}{\partial x} + v\frac{\partial T}{\partial y}\right) = k\left(\frac{\partial^2 T}{\partial x^2} + \frac{\partial^2 T}{\partial y^2}\right), \tag{4}$$

where c_p, k are heat capacity and thermal conductivity of the melt respectively.

To prescribe boundary conditions to equations (1)–(4), the symmetry about $x = 0$ (see Figure 1) allows to consider only the region where $x \geqslant 0$. Thus, the inlet velocity and temperature at $y = 0$ are given by

$$(u, v) = (0, V_c), \quad T = T_c, \tag{5}$$

and at the mould wall $x = W$,

$$k\frac{\partial T}{\partial x} = -Q,$$

where $Q > 0$ denotes a constant heat flux. In the axis of symmetry $x = 0$,

$$\frac{\partial T}{\partial x} = 0$$

and at the meniscus $h = h(x,t)$

$$\left(\frac{\partial T}{\partial x}, \frac{\partial T}{\partial y}\right) \cdot \left(-\frac{\partial h}{\partial x}, 1\right) = 0. \tag{6}$$

The initial condition at $t = 0$ is given by $T = T_c$.

Likewise, the shape of meniscus is the result of interaction between the pressure differences at the interface melt-air as mentioned by Bikerman [10], i.e.

$$-(p-p_a)=\gamma\,\frac{\partial^2 h/\partial x^2}{(1+(\partial h/\partial x)^2)^{3/2}}, \tag{7}$$

where p_a and γ denote the atmospheric pressure and surface tension coefficient between the melt and the air respectively. Also, the volume of liquid steel filling the mould at time t is given by

$$W\,V_c\,t=\int_0^W \big(h(x,t)-y_0\big)\,\mathrm{d}x. \tag{8}$$

3. Nondimensionalization

To obtain some key parameters in this cooling process, it is suitable to use the transformation

$$X=\frac{x}{W},\ Y=\frac{y}{W},\ \tau=\frac{V_c\,t}{W},\ H=\frac{h}{W},\ Y_0=\frac{y_0}{W},\ \theta=\frac{T-T_m}{T_c-T_m},\ U=\frac{u}{V_c},\ V=\frac{v}{V_c},\ P=\frac{p-p_a}{\rho\,g\,W},$$

where T_m is the melting temperature, i.e. at which the liquid steel becomes solid. From this, equations (1)–(3) becomes

$$\frac{\partial U}{\partial X}+\frac{\partial V}{\partial Y}=0,$$

$$\frac{\partial U}{\partial \tau}+U\frac{\partial U}{\partial X}+V\frac{\partial U}{\partial Y}=-\frac{1}{\mathrm{Fr}}\frac{\partial P}{\partial X}+\frac{1}{\mathrm{Re}}\left(\frac{\partial^2 U}{\partial X^2}+\frac{\partial^2 U}{\partial Y^2}\right), \tag{9}$$

$$\frac{\partial V}{\partial \tau}+U\frac{\partial V}{\partial X}+V\frac{\partial V}{\partial Y}=-\frac{1}{\mathrm{Fr}}\frac{\partial P}{\partial Y}+\frac{1}{\mathrm{Re}}\left(\frac{\partial^2 V}{\partial X^2}+\frac{\partial^2 V}{\partial Y^2}\right)-\frac{1}{\mathrm{Fr}} \tag{10}$$

and equation (4) becomes

$$\frac{\partial \theta}{\partial \tau}+U\frac{\partial \theta}{\partial X}+V\frac{\partial \theta}{\partial Y}=\frac{1}{\mathrm{Pe}}\left(\frac{\partial^2 \theta}{\partial X^2}+\frac{\partial^2 \theta}{\partial Y^2}\right), \tag{11}$$

where Re, Pe and Fr are the Reynolds, Peclet and Froude numbers given by

$$\mathrm{Re}=\rho\,V_c\,W/\mu,\quad \mathrm{Pe}=\rho\,c_p\,V_c\,W/k,\quad \mathrm{Fr}=V_c^2/(g\,W). \tag{12}$$

The boundary conditions (5)–(6), now become respectively

$$(U,V)=(0,1),\quad \theta=1, \tag{13}$$

$$\frac{\partial \theta}{\partial X}=-\beta, \tag{14}$$

$$\frac{\partial \theta}{\partial X}=0, \tag{15}$$

$$\left(\frac{\partial \theta}{\partial X},\frac{\partial \theta}{\partial Y}\right)\cdot\left(-\frac{\partial H}{\partial X},1\right)=0, \tag{16}$$

where $\beta=\frac{Q\,W}{k(T_c-T_m)}$. The initial condition at $\tau=0$ is $\theta=1$. Also, from (7),

$$\mathrm{Bo}(-P)=\frac{\partial^2 H/\partial X^2}{\big(1+(\partial H/\partial X)^2\big)^{3/2}}, \tag{17}$$

where Bo denotes the Bond number given by

$$\mathrm{Bo}=\frac{\rho\,g\,W^2}{\gamma}. \tag{18}$$

In addition, equation (8), now becomes

$$\tau=\int_0^1 \big(H(X,\tau)-Y_0\big)\,\mathrm{d}X. \tag{19}$$

4. Analysis

From the physical properties shown in Table 1, obtained from [1], the following key parameters are obtained: $\mathrm{Re}\approx 1000$, $\mathrm{Pe}\approx 200$, $\mathrm{Fr}\approx 10^{-4}$, $\mathrm{Bo}\approx 800$, according to (12) and (18).

Table 1. Values and description of parameters from [1].

Symbol	Value	Units	Description
ρ	8000	Kg m^{-3}	Density of liquid steel.
μ	0.0067	N m^{-2}	Viscosity of liquid steel.
c_p	500	J kg^{-1} K^{-1}	Heat capacity of liquid steel.
k	20	W m^{-1} K^{-1}	Thermal conductivity of liquid steel.
g	9.8	m s^{-2}	Constant of gravity.
T_c	1450	K	Casting temperature.
T_m	1400	K	Melting temperature.
V_c	0.01	m s^{-1}	Casting velocity.
γ	1880	N m^{-1}	Surface tension melt–air.
W	0.1	m	Mould width.
L	0.35	m	Mould height.

The parameters Re and Pe allow to determine the thickness of the momentum and thermal boundary layers: $\mathrm{Re}^{-1/2}$ and $\mathrm{Pe}^{-1/2}$ for the fluid flow and heat transfer respectively. Likewise, the key parameter Bo indicates that the thickness of the meniscus deviation is $\mathrm{Bo}^{-1/2}$ as shown in Figure 2 and the solidification point is located at $\tilde{P}$. In Figure 2, the thermal boundary layer is wider than the region wherein the meniscus deviates and two regions are determined: $1 - X \sim \mathrm{O}(\mathrm{Pe}^{-1/2})$ and $1 - X \sim \mathrm{O}(\mathrm{Bo}^{-1/2})$, also, far away of the thermal boundary layer one region wherein $1 - X \sim \mathrm{O}(1)$ is suitable to consider and thus, three regions will be analyzed.

4.1. $1 - X \sim \mathrm{O}(1)$

Since $\mathrm{Re} \gg 1$ and $\mathrm{Fr} \ll 1$, equations of momentum conservation (9), (10) at leading order become

$$\frac{\partial P}{\partial X} = 0, \quad \frac{\partial P}{\partial Y} = -1,$$

hence

$$P = -Y + f(\tau) \tag{20}$$

with a function f to be determined. On the meniscus $P = 0$ and $Y = H(X, \tau)$ and from (20), $H(X, \tau) = f(\tau)$. Using (19), $f(t) = Y_0 + \tau$, thus

$$H(X, \tau) = Y_0 + \tau,$$

which shows that in this region the shape of the meniscus is flat.

Also, since $\mathrm{Re} > \mathrm{Pe}$, the fluid flow is inviscid which implies that $U \sim 0$, $V \sim 1$ [1] and equation (11) is reduced to

$$\frac{\partial \theta}{\partial \tau} + \frac{\partial \theta}{\partial Y} = 0,$$

which gives $\theta = 1$ by the initial condition.

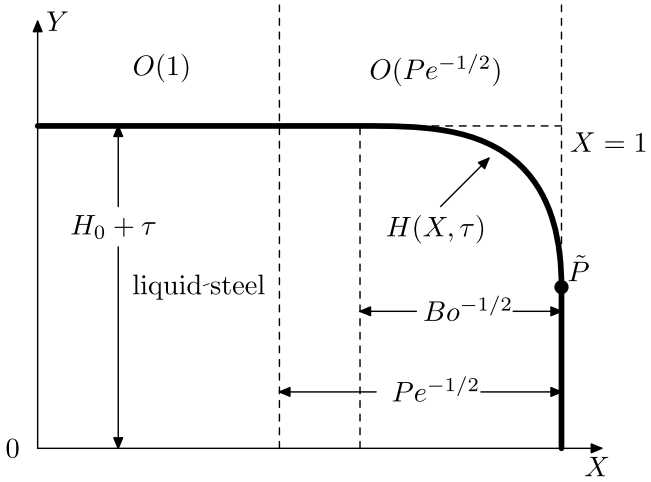

Fig. 2. The shape of the meniscus for $X \geqslant 0$. The flat shape is given by $H = H_0 + \tau$ para $H_0 = Y_0$ in the region $1 - X \sim \mathrm{O}(1)$, far away of the region $1 - X \sim \mathrm{O}(\mathrm{Pe}^{-1/2})$. The region $1 - X \sim \mathrm{O}(\mathrm{Bo}^{-1/2})$ is where the meniscus deviates and the solidification point is located at $\tilde{P}$. Also, the mould wall is located at $X = 1$.

Likewise, the meniscus determined by the melt-air interface is a moving boundary which can be fixed using the *Boundary Immobilization Method* (BIM) [13] to avoid solving equation (11) in a moving-mesh domain; thus the transformation

$$\hat{X} = 1 - X, \quad \hat{Y} = \frac{Y}{Y_0 + \tau},$$

allows to obtain from (11)

$$\frac{\partial \theta}{\partial \tau} + \left(\frac{1 - \hat{Y}}{Y_0 + \tau}\right) \frac{\partial \theta}{\partial \hat{Y}} = \frac{1}{\mathrm{Pe}} \left(\frac{\partial^2 \theta}{\partial \hat{X}^2} + \frac{1}{(Y_0 + \tau)^2} \frac{\partial^2 \theta}{\partial \hat{Y}^2}\right) \tag{21}$$

in

$$\hat{R} = \{(\hat{X}, \hat{Y}) \,/\, 0 \leqslant \hat{X} \leqslant 1,\, 0 \leqslant \hat{Y} \leqslant 1\},$$

and the boundary conditions (13)–(16) become

$$\begin{aligned} \frac{\partial \theta}{\partial \hat{X}} &= \beta \quad \text{at} \quad \hat{X} = 0, \\ \frac{\partial \theta}{\partial \hat{X}} &= 0 \quad \text{at} \quad \hat{X} = 1, \\ \theta &= 1 \quad \text{at} \quad \hat{Y} = 0, \\ \frac{\partial \theta}{\partial \hat{Y}} &= 0 \quad \text{at} \quad \hat{Y} = 1 \end{aligned} \tag{22}$$

and the initial condition is $\theta = 1$ at $\tau = 0$.

4.2. $1 - X \sim \mathbf{O(Pe^{-1/2})}$

Using the transformation

$$\tilde{X} = \mathrm{Pe}^{1/2}(1 - X), \quad \tilde{Y} = \frac{Y}{Y_0 + \tau},$$

equation (11) becomes

$$\frac{\partial \theta}{\partial \tau} + \frac{1 - \tilde{Y}}{Y_0 + \tau} \frac{\partial \theta}{\partial \tilde{Y}} = \frac{\partial^2 \theta}{\partial \tilde{X}^2} + \frac{1}{\mathrm{Pe}(Y_0 + \tau)^2} \frac{\partial^2 \theta}{\partial \tilde{Y}^2} \tag{23}$$

in

$$\tilde{R} = \{(\tilde{X}, \tilde{Y}) \,/\, 0 \leqslant \tilde{X} < \infty,\, 0 \leqslant \tilde{Y} \leqslant 1\}.$$

with boundary conditions, from (13)–(16),

$$\begin{aligned} \frac{\partial \theta}{\partial \tilde{X}} &= \beta\, \mathrm{Pe}^{-1/2} \quad \text{at} \quad \tilde{X} = 0, \\ \theta &\to 1 \quad \text{as} \quad \tilde{X} \to \infty, \\ \theta &= 1 \quad \text{at} \quad \tilde{Y} = 0, \\ \frac{\partial \theta}{\partial \tilde{Y}} &= 0 \quad \text{at} \quad \tilde{Y} = 1 \end{aligned} \tag{24}$$

(25)

and initial condition $\theta = 1$ at $\tau = 0$.

Also, the fraction $1/(\mathrm{Pe}(Y_0 + \tau)^2)$ decreases the second term of the right hand side in equation (23) at the meniscus $\tilde{Y} = 1$, equation (23) becomes

$$\frac{\partial \theta}{\partial \tau} = \frac{\partial^2 \theta}{\partial \tilde{X}^2}, \tag{26}$$

in $0 < \tilde{X} < \infty$, which is subject to the boundary conditions

$$\frac{\partial \theta}{\partial \tilde{X}} = \tilde{Q} \quad \text{at} \quad \tilde{X} = 0,$$

where $\tilde{Q} = \beta\, \mathrm{Pe}^{-1/2}$ and

$$\theta \to 1 \quad \text{as} \quad \tilde{X} \to \infty$$

and initial condition $\theta = 1$ at $\tau = 0$.

Thus, the solution to the equation (26) was obtained by Vynnycky et al. [1] and it can be expressed by

$$\tilde{\theta}(\tilde{X}, \tau) = 1 + \tilde{Q} \left(\tilde{X}\, \mathrm{erfc} \left\{ \frac{\tilde{X}}{2\sqrt{\tau}} \right\} - 2\sqrt{\frac{\tau}{\pi}}\, \exp \left\{ -\frac{\tilde{X}^2}{4\tau} \right\} \right). \tag{27}$$

Now, the temperature at the mould wall is obtained from (27) at $\tilde{X} = 0$,

$$\tilde{\theta}(0, \tau) = 1 - \tilde{Q} \frac{2\sqrt{\tau}}{\sqrt{\pi}}.$$

and for the necessary time to fill the mould, $t = t^*$, $L = y_0 + V_c\, t^*$ or $\tau^* = L/W - Y_0$ and the temperature at the solidification point $\tilde{P}$ is zero, for which,

$$0 = \tilde{\theta}(0, \tau^*) = 1 - \tilde{Q}\frac{2\sqrt{L/W - Y_0}}{\sqrt{\pi}} \quad \text{or} \quad \tilde{Q} = \frac{\sqrt{\pi}}{2\sqrt{\frac{L}{W} - Y_0}}.$$

4.3. $1 - X \sim \mathbf{O(Bo^{-1/2})}$

Using the transformation

$$\bar{X} = \mathrm{Bo}^{1/2}(1 - X), \quad \bar{Y} = \mathrm{Bo}^{1/2}(Y_0 + \tau - Y), \tag{28}$$

the region to obtain θ is defined by

$$\bar{R} = \{(\bar{X}, \bar{Y}) \,/\, 0 \leqslant \bar{X} < \infty,\, \bar{H}(\bar{X}, \tau) \leqslant \bar{Y} < \infty\},$$

where $\bar{H}$ can be obtained from (28) to satisfy

$$Y_0 + \tau - H = \mathrm{Bo}^{-1/2}\bar{H},$$

and from equation (17),

$$\bar{H} = \frac{\partial^2 \bar{H}/\partial \bar{X}^2}{\left(1 + (\partial^2 \bar{H}/\partial \bar{X}^2)^2\right)^{3/2}},$$

which was solved by Vynnycky et al. in [1] with the shape of meniscus, given by

$$\bar{X} = \bar{X}_0 - \left[\sqrt{4 - \bar{H}^2} - \ln\frac{2 + \sqrt{4 - \bar{H}^2}}{\bar{H}}\right], \tag{29}$$

where $\bar{X}_0 = \sqrt{2} - \ln(1 + \sqrt{2})$.

On the other hand, equation (11) using (28) becomes

$$\frac{\partial \theta}{\partial \tau} = \frac{\mathrm{Bo}}{\mathrm{Pe}}\left(\frac{\partial^2 \theta}{\partial \bar{X}^2} + \frac{\partial^2 \theta}{\partial \bar{Y}^2}\right) \tag{30}$$

for $(\bar{X}, \bar{Y}) \in \bar{R}$ and subject to boundary conditions, from (13)–(16)

$$\frac{\partial \theta}{\partial \bar{X}} = \beta\,\mathrm{Bo}^{-1/2} \quad \text{at} \quad \bar{X} = 0, \tag{31}$$

$$\theta \to 1 \quad \text{as} \quad \bar{X} \to \infty,$$

$$\theta \to 1 \quad \text{as} \quad \bar{Y} \to \infty,$$

$$\theta = \tilde{\theta}(\tilde{X}, \tau) \quad \text{at} \quad \bar{Y} = \bar{H}(\bar{X}, \tau).$$

and the initial condition $\theta = 1$ at $\tau = 0$.

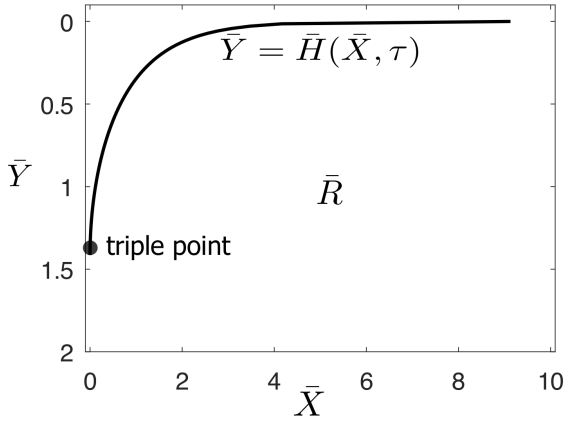

Fig. 3. Shape of the meniscus adjacent to the mould wall in $\bar{X} - \bar{Y}$ coordinates; the solidification point is located wherein the *triple point* is pointed out.

Figure 3 shows the shape of meniscus adjacent to the mould wall given by equation (29) in $\bar{X} - \bar{Y}$ coordinates; the solidification point is pointed out as *triple point* in figure and is located at $\bar{Y} = \bar{H} = \sqrt{2}$ wherein three interfaces are present melt-air, solid wall-melt and solid wall-air [1].

5. Numerics

Equations (21), (23) and (30) were solved in three regions: $\hat{R}$, $\tilde{R}$ and $\bar{R}$ respectively using the C++ solver *OpenFOAM* [14]. OpenFOAM, using the *finite volume method* (FVM) [15] obtains the numerical solution of equations (21), (23) and (30) but beforehand, it builds a discretization via a meshing of the regions $\hat{R}$, $\tilde{R}$ and $\bar{R}$ using an utility contained in OpenFOAM called *blockMesh*, designed to carry out this task.

5.1. In the region $\hat{R} = [0,1] \times [0,1]$

The utility blockMesh built the mesh for the region $\hat{R}$, which is shown in Figure 4, in this case the solidification point is located at $(\hat{X}, \hat{Y}) = (0,1)$ and the temperature at this point will be denoted by $\theta_{\hat{R}}$. Also, the mould wall is located at $\hat{X} = 0$. The mesh built is formed by $N_{\hat{X}} \times N_{\hat{Y}} = 50 \times 50 = 2500$ blocks, where $N_{\hat{X}}$, $N_{\hat{Y}}$ denote the number of blocks in $\hat{X}$- and $\hat{Y}$-axis respectively.

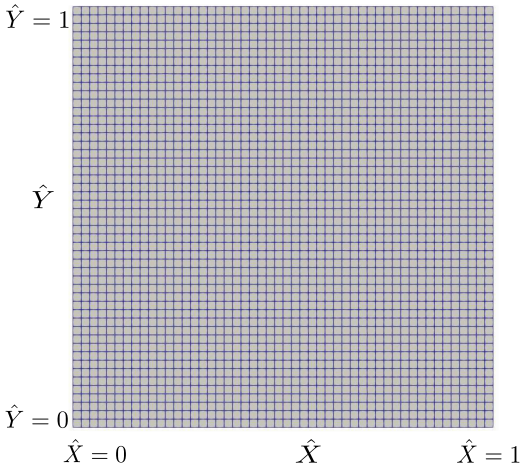

Fig. 4. Mesh for the region $\hat{R}$. The solidification point is located $(\hat{X}, \hat{Y}) = (0,1)$.

5.2. In the region $\tilde{R}$

The mesh for this region was built by the utility blockMesh as shown in Figure 5. To represent the boundary condition $\theta \to 1$ as $\tilde{X} \to \infty$, it was necessary to set $\tilde{X}_\infty$ as a large number and thus, $\theta \to 1$ as $\tilde{X} \to \tilde{X}_\infty$. Likewise, the solidification point is located at $(\tilde{X}, \tilde{Y}) = (0,1)$ and the temperature at this point will be denoted by $\theta_{\tilde{R}}$.

The mesh built is formed by $N_{\tilde{X}} \times N_{\tilde{Y}} = 180 \times 20 = 1600$ blocks, where $N_{\tilde{X}}$, $N_{\tilde{Y}}$ denote the number of blocks in $\tilde{X}$- and $\tilde{Y}$-axis respectively. Also, the setting $\bar{X}_\infty \sim 9$ was large enough because in the $\tilde{X}$-axis, the erf-function decays exponentially.

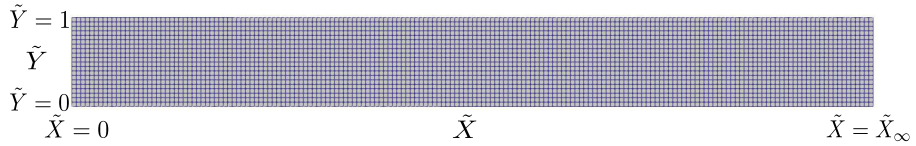

Fig. 5. Mesh for the region $\tilde{R}$. The solidification point is located at $(\tilde{X}, \tilde{Y}) = (0,1)$.

5.3. In the region $\bar{R}$

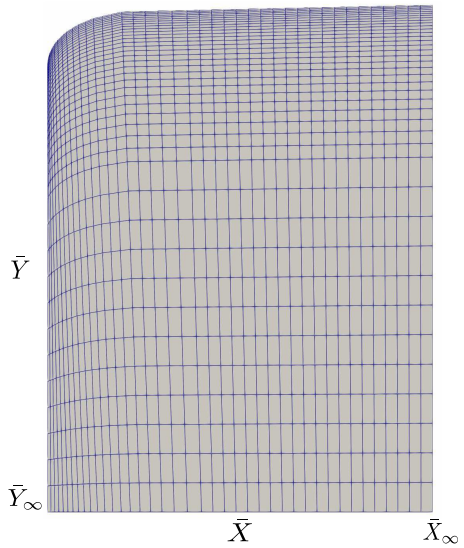

Fig. 6. Mesh built by blockMesh utility to solve equation (30) using the volume-finite method.

In Figure 6 is shown the mesh for the region $\bar{R}$ built by blockMesh. As shown, blockMesh is capable to construct meshes wherein there exists a curve-shaped boundary as it was obtained by the meniscus near to the mould wall. Likewise, in this region, the solidification point is located at $(\bar{X}, \bar{Y}) = (0, \sqrt{2})$ and the temperature at this point will be denoted by $\theta_{\bar{R}}$. The mesh built is formed by $N_{\bar{X}} \times N_{\bar{Y}} = 40 \times 40 = 1600$ blocks, where $N_{\bar{X}}$, $N_{\bar{Y}}$ denote the number of blocks in $\bar{X}$- and $\bar{Y}$-axis respectively. Also, the setting $\bar{X}_\infty \sim 9$ and $\bar{Y}_\infty \sim 12$ was enough due to that the erf-function decays exponentially.

6. Results

To perform computations to obtain the numerical solution of the equations (21), (23) and (30), it is necessary to define the boundary conditions that must be prescribed at the mould wall. Hence, from equation (22), $\hat{Q} = \beta$ is prescribed with $\hat{Q} = -6.7090$. Figures 7 and 8 show the $\theta-$values by solving equation (21). In Figure 7 the region of the liquid steel at $\tau = 0.5$ and $\tau = 1.0$ show a narrow region where θ-value has changed, whereas in Figure 8 the θ-values at $\tau = 2.0$ and $\tau = 3.5$ show lower θ-values and the onset of the solidification emerges at $\tau = \tau^* = 3.5$, thus, by setting $\theta_{\hat{R}}(\tau) = \theta(0,1,\tau)$, it is clear that $\lim_{\tau \to \tau^*} \theta_{\hat{R}}(\tau) = 0$.

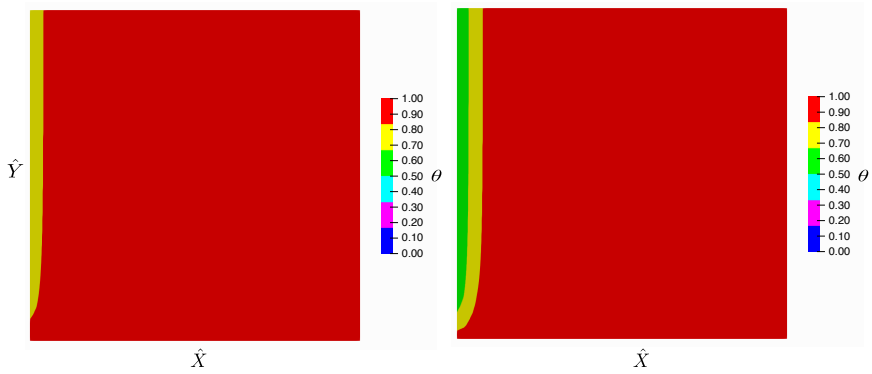

Fig. 7. θ-values at $\tau = 0.5$ (left) and $\tau = 1.0$ (right) obtained by solving equation (21).

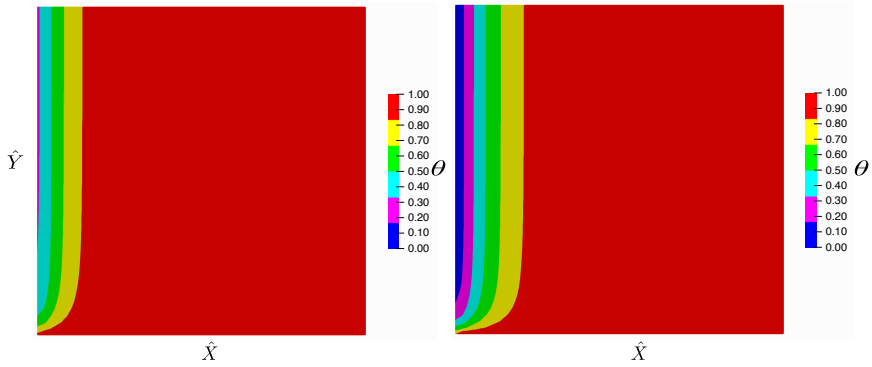

Fig. 8. $\theta-$values at $\tau = 2.0$ (left) and $\tau = 3.5$ (right) obtained by solving equation (21).

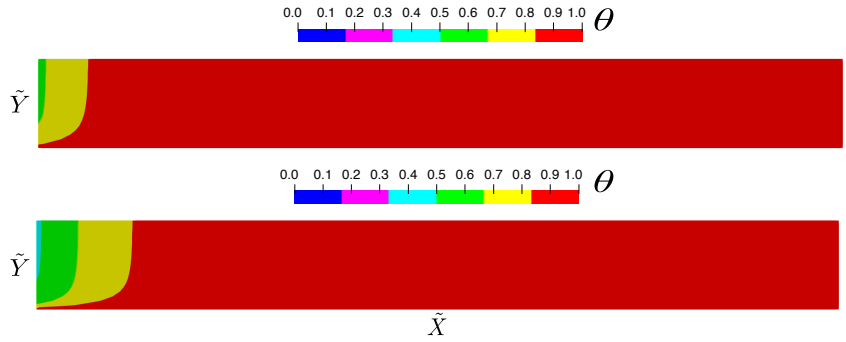

Fig. 9. θ-values at $\tau = 0.5$ (up), $\tau = 1.0$ (down) obtained by solving equation (23).

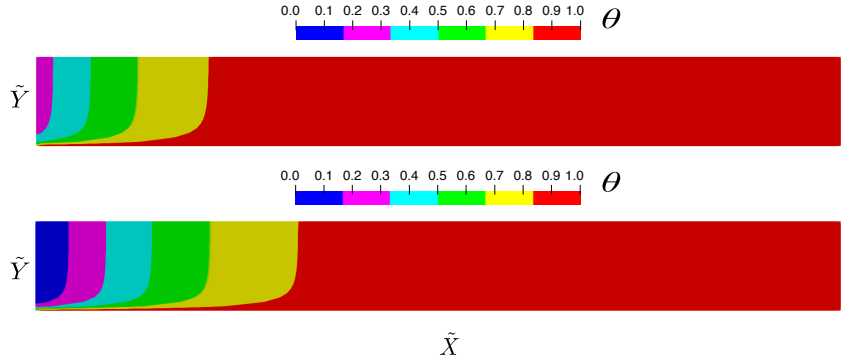

Fig. 10. θ-values at $\tau = 2.0$ (up), $\tau = 3.5$ (down) obtained by solving equation (23).

Also, for equation (23), the boundary condition (24) is set for $\tilde{Q} = \beta \operatorname{Pe}^{-1/2}$ with $\tilde{Q} = -0.4744$ and the θ-values were obtained by solving numerically equation (23) and are shown in Figures 9 and 10. In Figure 9 are shown the θ-values at $\tau = 0.5$ and $\tau = 1.0$ whereas in Figure 10 are shown the θ-values at $\tau = 2.0$ and $\tau = \tau^* = 3.5$, and again, by setting $\theta_{\tilde{R}} = \theta(0, 1, \tau)$ it is clear that $\lim\limits_{\tau \to \tau^*} \theta_{\tilde{R}}(\tau) = 0$, which indicates the onset of the solidification once $\tau = \tau^*$.

The numerical solution for equations (21) and (23) converges to $\theta = 0$ as $\tau \to \tau^*$ at $(\hat{X}, \hat{Y}) = (0, 1)$ and $(\tilde{X}, \tilde{Y}) = (0, 1)$ respectively. These points in the regions $\hat{R}$ and $\tilde{R}$ correspond to the solidification point beforehand mentioned.

For the solution of equation (30), the boundary condition (31) is prescribed by setting $\bar{Q} = \beta\,\mathrm{Bo}^{-1/2}$ with $\bar{Q} = -0.23719$ and hence by solving equation (30), the θ-values were obtained numerically and these are shown in Figures 11 and 12.

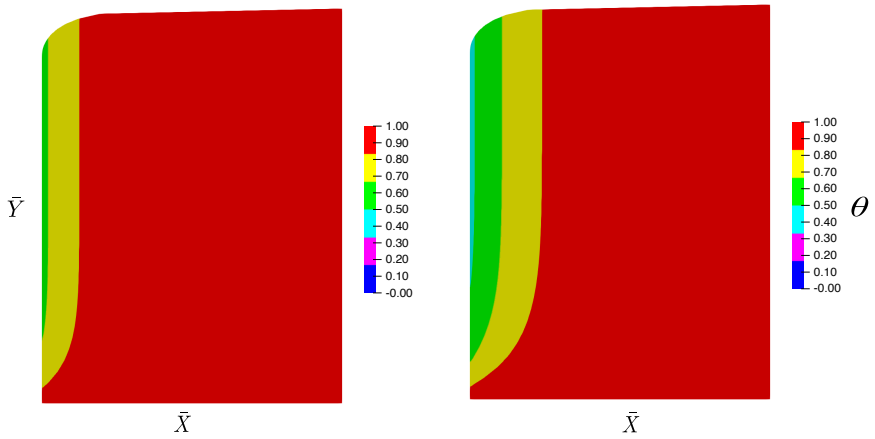

Fig. 11. θ-values at $\tau = 0.5$ (left), $\tau = 1.0$ (right) obtained by solving equation (30).

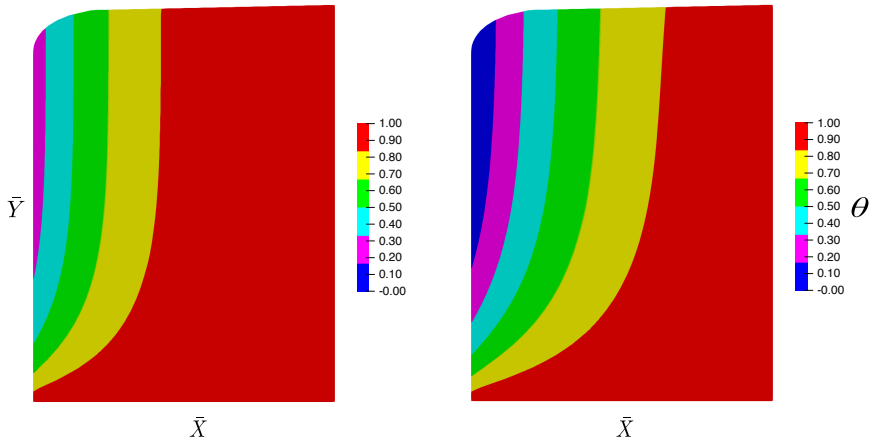

Fig. 12. θ-values at $\tau = 2.0$ (left), $\tau = 3.5$ (right) obtained by solving equation (30).

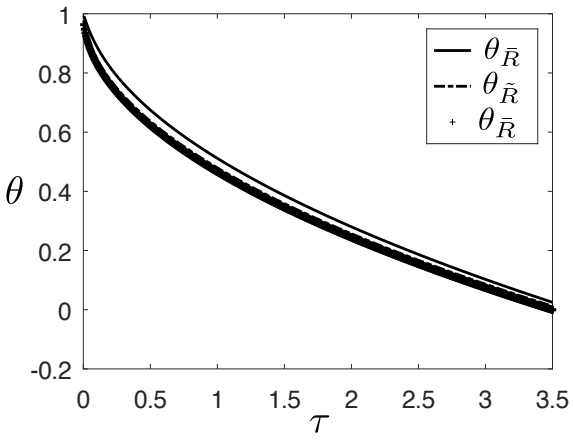

Fig. 13. θ-values for regions $\hat{R}$, $\tilde{R}$ and $\bar{R}$ at the solidification point.

In Figure 11, the θ-values are shown at $\tau = 0.5$ and $\tau = 1.0$ wherein the region of the liquid steel adjacent to the mould wall starts the cooling process and only a narrow region shows differences in the θ-values, whereas in Figure 12 are shown the $\theta-$values at $\tau = 2.0$ and $\tau = \tau^* = 3.5$ for which this cooling process is more evident. Hence, at $\tau = \tau^*$ the onset of solidification begins at the solidification point $(\bar{X}, \bar{Y}) = (0, \sqrt{2})$ and by setting $\theta_{\bar{R}}(\tau) = \theta(0, \sqrt{2}, \tau)$, the solution obtained shows that

$$\lim_{\tau \to \tau^*} \theta_{\bar{R}}(\tau) = 0.$$

Finally, as $\tau \to \tau^*$, $\theta_{\hat{R}}, \theta_{\tilde{R}}$ and $\theta_{\bar{R}}$ converges to zero at the solidification point as shown in Figure 13, thus at this point can be observed that $\theta(\tau_1) > \theta(\tau_2)$ when $\tau_1 < \tau_2$ with $\tau_i > 0$ for $i = 1, 2$.

7. Discussion and conclusion

In this article, it was studied the temperature of the melt at the solidification point in ingot casting processes that has determined the onset of the solidification process as shown in Figures 8, 10 and 12. At this solidification point there exists the lowest θ-value in regions in the regions $\hat{R}$, $\tilde{R}$ and $\bar{R}$ and this fact was verified by obtaining the numerical solution of equations (21), (23) and (30).

Using asymptotic techniques enables to reduce systematically equation (11) to obtain an ordinary differential equation (26) with solution determined the profile of the temperature of the meniscus, starting at the solidification point adjacent to the mould wall wherein the onset of the solidification for the steel begins. Thus, this profile allowed to compute the heat flux $\tilde{Q}$ necessary to fill the mould with liquid steel before it solidifies.

Likewise, to split the whole domain in which the liquid steel occupies in the mould into three regions: $\hat{R}$, $\tilde{R}$ and $\bar{R}$ wherein equations (21), (23) and (30) rule the heat transfer and allowed to obtain several features of the cooling process of the melt via the analysis given for $1 - X \sim \mathrm{O}(1)$, $1 - X \sim \mathrm{O}(\mathrm{Pe}^{-1/2})$ and $1 - X \sim \mathrm{O}(\mathrm{Bo}^{-1/2})$ respectively.

In this research, a technique known as *Boundary Immobilization Method* (BIM) was used to set the upper boundary of the regions $\hat{R}$ and $\tilde{R}$ to a fixed position due to the rising level of meniscus by the incoming liquid steel in the mould. Hence, for equations (21) and (23), the upper boundaries at $\hat{Y} = 1$ and $\tilde{Y} = 1$ respectively were considered. This method (BIM) also was applied in problems related to free and moving boundary problems wherein there exist two phases solid and liquid steel [13, 16] or one-phase problems with solidification or melting [13, 17].

Around the solidification point the shape of the meniscus is not flat as pointed out in [2, 4, 5] and is similar to that found in continuous casting processes wherein a combination of moving mould wall and heat transfer determine the solidification point of the steel [6, 7, 9].

Although inside of the mould from $\tau = 0$ upto $\tau = \tau^*$ there exist two fluids (melt and air) and the problem can be treated using the techniques used for multiphase flows as described by Prosperetti et al. [18], in this article, the BIM technique allowed to consider only one region and from this the problem can be treated using several techniques as the finite differences method [19, 20] in regions $\hat{R}$ and $\tilde{R}$ or the finite volume method [15] for the regions $\hat{R}$, $\tilde{R}$ and $\bar{R}$ as was done in this research.

Finally, the OpenFOAM software was employed to obtain the numerical solution of equations (21), (23) and (30) using pre-existing solvers as *laplacianFoam* [14, 21] but it is suitable to mention that equations wherein there exist a free or a moving boundary problem as emerges when the liquid steel becomes solid can be treated to obtain the numerical solution using either the OpenFOAM software or GNU-Octave [22] with an algorithm based on the finite difference method as described in [23–25].

[1] Vynnycky M., Zambrano M., Cuminato J. A. On the avoidance of ripple-marks on cast metal surfaces. International Journal of Heat and Mass Transfer. **86**, 43–54 (2015).

[2] Wray P. J. Geometric features of chill-cast surfaces. Metallurgical Transactions B. **12**, 167–176 (1981).

[3] Tomono H., Kurz W., Heinemann W. The liquid steel meniscus in molds and its relevance to the surface quality of casting. Metallurgical Transactions B. **12**, 409–411 (1981).

[4] Jacobi H., Schwerdfeger K. Ripple marks on cast steel surfaces. ISIJ International. **53** (7), 1180–1196 (2013).

[5] Fredriksson H., Elfsberg J. Thoughts about the initial solidification process during continuous casting of steel. Scandinavian Journal of Metallurgy. **31** (5), 292–297 (2002).

[6] Takeuchi E., Brimacombe J. K. The formation of oscillation marks in the continuous casting of steel slabs. Metallurgical Transactions B. **15**, 493–509 (1984).

[7] Steinrück H., Rudisher C., Schneider W. Modelling of continuous casting process. Nonlinear Analysis: Theory, Methods & Applications. **30** (8), 4915–4925 (1997).

[8] Schwerdtfeger K., Sha H. Depth of oscillation marks forming in continuous casting of steel. Metallurgical and Materials Transactions B. **31**, 813–826 (2000).

[9] Vynnycky M., Zambrano M. Towards a "moving-point" formulation for the modelling of oscillation-mark formation in the continuous casting of steel. Applied Mathematical Modelling. **63**, 243–265 (2018).

[10] Bikerman J. Physical Surfaces. Elsevier Science (2012).

[11] Pletcher R. Computational Fluid Mechanics and Heat Transfer. CRC Press (1997).

[12] Dantzig J., Tucker C. Modeling in Material Processing. Cambridge University Press (2012).

[13] Crank J. Free and Moving Boundary Problems. Oxford University Press (1975).

[14] Elsevier Science. OpenFOAM — Field Operation and Manipulation. OpenFOAM foundation (2012).

[15] Leveque J. R. Finite Volume Methods for Hyperbolic Problems. Cambridge University Press (2002).

[16] Mitchell S. L., Vynnycky M. On the numerical solution of two-phase Stefan problems with heat-flux boundary conditions. Journal of Computational and Applied Mathematics. **264**, 49–64 (2014).

[17] Mitchell S. L., Vynnycky M. Finite-difference methods with increased accuracy and correct initialization for one-dimensional Stefan problems. Applied Mathematics and Computation. **215** (4), 1609–1621 (2009).

[18] Prosperetti A., Tryggvason G. Computational Methods in Multiphase Flow. Cambridge University Press (2009).

[19] Burden R., Faires J. Numerical Analysis. Brooks/Cole (2012).

[20] Leveque R. J. Finite Difference Methods for Ordinary and Partial Differential Equations. Society for Industrial and Applied Mathematics (SIAM) (2007).

[21] Chen G., Xiong Q., Morris P., Paterson E., Sergeev A., Wang Y. OpenFOAM for Computational Fluid Dynamics. Notices of the AMS. **61** (4), 354–363 (2014).

[22] Eaton J., Bateman D., Hauberg S., Wehbring R. GNU Octave, version 5.2.0 manual: a high-level interactive language for numerical computations. `https://www.gnu.org/software/octave/doc/v5.2.0` (2020).

[23] Caldwell J., Kwan Y. Y. Numerical methods for one-dimensional Stefan problems. Communications in Numerical Methods in Engineering. **20** (7), 535–545 (2004).

[24] Voller V. R. Fast Implicit Finite-Difference Method for the Analysis of Phase Change Problems. Numerical Heat Transfer, Part B: Fundamentals. **17** (2), 155–169 (1990).

[25] Voller V. R., Prakash C. A fixed grid numerical modelling methodology for convection-diffusion mushy region phase-change problems. International Journal of Heat and Mass Transfer. **30** (8), 1709–1719 (1987).

Чисельна оцінка температури точки затвердіння в процесах лиття зливків

Замбрано М.

Національний університет Барранки, Барранка, 15169, Ліма, Перу

Аналіз для чисельного обчислення температури біля точки затвердіння рідкої сталі або розплаву, що міститься у формі, здійснюється через взаємодію рівнянь збереження маси, імпульсу та теплопередачі. За допомогою асимптотичних методів проаналізовано процес охолодження рідкої сталі за рахунок відведення тепла через стінки форми та отримано звичайне диференціальне рівняння, яке описує температуру межі розплав–повітря. Крім того, температура розплаву у формі навколо точки затвердіння обчислюється чисельно за допомогою програмного забезпечення OpenFOAM.

Ключові слова: *точка затвердіння; процес охолодження; асимптотичні методи; звичайне диференціальне рівняння.*